Journal of Computational Physics 292 (2015) 272–286

Contents lists available at ScienceDirect

Journal of Computational Physics

www.elsevier.com/locate/jcp

A high resolution differential filter for large eddy simulation: Toward explicit filtering on unstructured grids

A. Najafi-Yazdi [a,b,*], M. Najafi-Yazdi [a], L. Mongeau [a]

[a] Department of Mechanical Engineering, McGill University, Macdonald Engineering Building, 817 Sherbrooke Street West, Montreal, QC, H3A 0C3, Canada
[b] Anyon Systems Inc., Montreal, QC, H9P 1G9, Canada

ARTICLE INFO

Article history:
Received 3 July 2014
Received in revised form 23 February 2015
Accepted 18 March 2015
Available online 28 March 2015

Keywords:
Large eddy simulation
Approximate deconvolution modeling
Explicit filtering
Unstructured grids

ABSTRACT

A high resolution, low-pass differential filter for numerical simulations on unstructured grids is proposed. The finite element discretization of the filter equation on a structured grid results in a discrete compact filter. The proposed filter is significantly less dissipative than Germano's differential filter, while completely suppresses fluctuations at the grid cut-off frequency. Manufactured solutions were used to verify the performance of the proposed filter. The results suggest that the proposed filter will be very effective for explicit filtering and approximate deconvolution modeling in Large Eddy Simulations.

1. Introduction

Large Eddy Simulation (LES) of turbulent flows has found widespread applications both in academia and industry. The idea behind Large Eddy Simulations (LES) is to decompose the flow properties into a large-scale or resolved component, $\overline{\phi}$, and a small-scale or subgrid component, ϕ_{sg} [1]. This decomposition is achieved by applying a low pass, spatial filter. The filter width usually corresponds to the smallest scale resolved on the grid.

It is customary to *implicitly* apply the filter by solving the filtered Navier–Stokes equations with a presumed subgrid-scale stress model. This procedure is known as *implicit filtering* [2]. In implicit filtering, the filter function is not necessarily known as it is implicitly defined by the subgrid model and the numerical grid [2–4]. Implicit filters, therefore, do not allow the control of numerical errors caused by truncation errors and aliasing of high frequencies [5]. Moreover, the filter spectral distribution and its energy dissipation cannot be quantified [2,6,7].

These problems can be addressed by using LES methodologies based on *explicit filtering* of the flow field, namely the Approximate Deconvolution Model (ADM) [7–10], and the relaxation filtering (RF) technique [11–16]. In these methods, filtering is an explicit part of the numerical simulation to prevent the energy accumulation at the grid cut-off. Since the filter operator is known, the energy dissipation associated with filtering can be quantified. So far, successful applications of these methods have only been reported on structured grids, for which a discrete high-order filter operator can be easily constructed. Examples include the use of Lele's compact filters [17] by Visbal and Rizetta [18], Rizzeta et al. [19], Uzun and Hussaini [20,21], as well as explicit discrete filters by Bogey and Bailly [12,13], Berland et al. [15], and Fauconnier et al. [16].

* Corresponding author. Fax: +1 514 398 7365.
E-mail addresses: alireza.najafiyazdi@mail.mcgill.ca, ayazdi@anyonsys.com (A. Najafi-Yazdi), mostafa.najafiyazdi@mail.mcgill.ca (M. Najafi-Yazdi), luc.mongeau@mcgill.ca (L. Mongeau).

http://dx.doi.org/10.1016/j.jcp.2015.03.034
0021-9991/

Nomenclature

h	Local filter width
$\mathbf{J}$	Jacobian matrix
k	Magnitude of wavenumber
$\mathbf{k}$	Three dimensional wavenumber vector
m_{ij}	Component of filter left-hand-side mass matrix
n_{ij}	Component of filter right-hand-side mass matrix
N_j	Shape function for local node j
$T(\mathbf{k})$	Filter transfer function
x, y	Spatial coordinates in the physical space
Greek	
α	Filter parameter for filter cut-off frequency in the computational space
α_{ij}	Components of filter cut-off frequency parameter in the physical space
α_f	Filter parameter for compact notation
β	Filter parameter for grid cut-off frequency in the computational space
β_{ij}	Components of grid cut-off frequency parameter in the physical space
δ	Germano's filter radius
ϕ	Unfiltered scalar variable
$\overline{\phi}$	Filtered scalar variable
ξ, η	Spatial coordinates in the two-dimensional computational space
Ω	Arbitrary element in the physical space
$\widetilde{\Omega}$	Transformed element in the computational space, a.k.a. reference element
Subscript	
cnt	Continuous
fc	Filter cut-off
g	Grid cut-off
Gr	Germano's

The extension of discrete filter operators to unstructured grids is not straightforward which has hampered the use of ADM and RF for LES on unstructured grids. Marsden et al. [22] and Haselbacher and Vasilyev [23] suggested explicit filtering procedures for unstructured grids based on a weighted sum of neighbouring node values. Both of these methods have drawbacks which have hampered their application. In particular, it is not possible to ensure the stability of the filter operator (i.e. $G(k) \leq 1, \forall k$) in a general mesh topology. Moreover, the spectral distribution of the filter kernel is strongly dependent on the distribution of surrounding nodes. The filter of Marsden et al. [22] also requires the careful selection of a subset of neighbouring nodes which might not exist in the presence of skewed and stretched elements [24].

Another approach for the design of discrete filter kernels is the use of differential operators. First introduced in the 1980's by Germano [25,26], differential filters for LES applications have been used by Mullen and Fischer [27], You et al. [28], and Bose et al. [24] Germano's differential filter is defined by the following differential equation:

$$\overline{\phi} - \delta^2 \frac{\partial^2 \overline{\phi}}{\partial x_j \partial x_j} = \phi \,, \tag{1}$$

where ϕ and $\overline{\phi}$ are unfiltered and filtered variables, respectively, and the filtering parameter, δ, controls the filter's attenuation. Germano's filter transfer function in the Fourier domain is given by

$$T_{Gr}(k) = \frac{1}{1 + \delta^2 k^2} \,, \tag{2}$$

where k is the wavenumber. Germano's filter is stable (i.e. $|T_{\mathrm{Gr}}| \leq 1$) for all values of wavenumber, and is a useful tool for theoretical analysis [29]. However, Germano's filter has some limitations for practical applications in LES. In particular, its transfer function, Eq. (2), never reaches zero in the discrete form. Therefore, Germano's filter does not completely remove the energy content of the subgrid scales. This means that Germano's filter, if used without any additional dissipation or subgrid model, cannot prevent energy accumulation near the grid cut-off, which eventually destabilizes the numerical simulation. Moreover, Germano's filter is rather dissipative at low to moderate wavenumbers, corresponding to resolved scales.

The aforementioned shortcomings of Germano's filter are addressed by a new differential filter proposed in this paper. The transfer function of the filter is designed to remain close to unity over a wide range of wavenumbers, resulting in minimal dissipation over resolved scales, and to decline sharply to zero near the grid cut-off in order to completely remove the subgrid energy content.

The paper is organized as follows. A brief discussion of the definition of grid cut-off wavenumber is provided in Section 2. The new filter is introduced in Section 3. In Section 4, it is shown that a Galerkin discretization of the filter in one dimension results in the second order compact filter introduced by Lele [17]. The spectral accuracy of the proposed filter is compared with that of other conventionally used models in Section 5. The derivation of the filter for two-dimensional triangular elements is presented in Section 6. In Section 7, numerical examples are used to illustrate the characteristics of the proposed filter. Conclusions are drawn in Section 8.

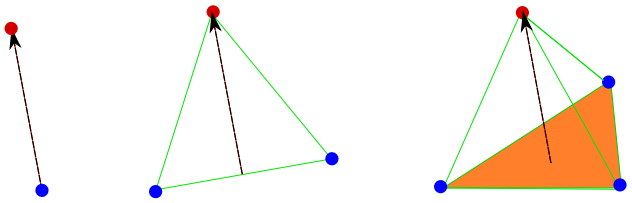

Fig. 1. Concept of grid cut-off in unstructured grids: a field quantity, ϕ, has a phase difference of π between the red node and the blue nodes on the opposite face in a (a) one-dimensional element; (b) two-dimensional triangular element; and (c) three-dimensional tetrahedron element. (For interpretation of the references to colour in this figure legend, the reader is referred to the web version of this article.)

2. Grid cut-off wavenumber and saw-tooth waves

The cut-off wavenumber corresponds to the highest wavenumber that can be resolved on a given computational grid. In effect, this corresponds to node to node oscillations in a structured grid. Waves with such characteristics are commonly referred to as *wiggles*, saw-tooth waves and q-waves [30] in the literature.

For structured grids, saw-tooth waves correspond to waves for which $k\Delta_\xi = \pi$, where Δ_ξ is the grid spacing in the computational domain. Similarly, saw-tooth waves in a simplicial element in unstructured grids can be characterized by a phase difference equal to π between any node and its opposite face. This description is schematically illustrated in Fig. 1, where a field quantity ϕ has a phase difference of π between the red node and the blue nodes on the opposite face. This means that a saw-tooth wave has a wavenumber which corresponds to $|\mathbf{k}\cdot\boldsymbol{\Delta}| = \pi$ where $\Delta = |\boldsymbol{\Delta}|$ is the distance between the red node and its opposite face.

3. Proposed differential filter

Following Germano's earlier work [26], a filter in the form of an elliptic partial differential equation (PDE) is considered. The filter equation is expected to be consistent for use with both structured and unstructured grids. Given spatial non-uniformities in unstructured grids, the elliptic PDE is expected to have a non-isotropic form in the physical domain. It should, however, reduce to an isotropic PDE for a uniform grid, or if it is recast in terms of the computational domain coordinates.

The new filter is proposed to take the following form in the physical domain:

$$\frac{\bar{\phi}}{\Delta} + \frac{\partial}{\partial x_i}\left(\alpha_{ij}^2 \Delta \frac{\partial \bar{\phi}}{\partial x_j}\right) = \frac{\phi}{\Delta} + \frac{\partial}{\partial x_i}\left(\beta_{ij}^2 \Delta \frac{\partial \phi}{\partial x_j}\right), \tag{3}$$

where Δ is related to the local filter width.

Considering uniform elements in the computational space,[1] the filter equation is expected to reduce to the following equation in the computational domain:

$$\bar{\phi} + \frac{\partial}{\partial \xi_j}\left(\alpha^2 \frac{\partial \bar{\phi}}{\partial \xi_j}\right) = \phi + \frac{\partial}{\partial \xi_j}\left(\beta^2 \frac{\partial \phi}{\partial \xi_j}\right). \tag{4}$$

Nondimensional parameters α and β are determined such that the filter transfer function, $T(k)$, satisfies

$$T(k_{1/2}) = \frac{1}{2}, \tag{5}$$

and

$$T(k_c) = 0, \tag{6}$$

for chosen values of $k_{1/2}$ and k_c. Through out this paper, $k_{1/2}$ is referred to as *filter* cut-off wavenumber, while k_c is referred to as *grid* cut-off wavenumber. The latter constraint, Eq. (6), enhances the numerical stability of the simulation by removing non-physical sawtooth waves which are typical of high order LES.

In what follows, a finite element discretization of Eq. (3) is utilized to determine filter coefficients. Relations between the filter coefficients in the physical domain, α_{ij} and β_{ij}, and those in the computation domain, *i.e.* α and β are also established.

4. The one-dimensional filter equation

Considering piecewise constant values for the filter coefficients α and β, and utilizing a finite element Galerkin projection, with one-dimensional linear elements, the filter equation in the computational domain, Eq. (4), is discretized around a given node i to obtain

[1] For unstructured grids, the computational space is considered to be the space within which *standard* elements are defined.

$$\frac{1}{6}\left(\bar{\phi}_{i-1}+4\bar{\phi}_i+\bar{\phi}_{i+1}\right)+\alpha^2\left(\bar{\phi}_{i-1}-2\bar{\phi}_i+\bar{\phi}_{i+1}\right)=\frac{1}{6}\left(\phi_{i-1}+4\phi_i+\phi_{i+1}\right)+\beta^2\left(\phi_{i-1}-2\phi_i+\phi_{i+1}\right). \tag{7}$$

Eq. (7) can be recast as

$$\alpha_f\bar{\phi}_{i-1}+\bar{\phi}_i+\alpha_f\bar{\phi}_{i+1}=a\phi_i+\frac{b}{2}\left(\phi_{i+1}+\phi_{i-1}\right), \tag{8}$$

where

$$\alpha_f=\frac{\frac{1}{6}+\alpha^2}{\frac{4}{6}-2\alpha^2}, \tag{9}$$

$$a=\frac{\frac{1}{3}-\beta^2}{\frac{1}{3}-\alpha^2}, \tag{10}$$

and

$$b=\frac{\frac{1}{6}+\beta^2}{\frac{1}{3}-\alpha^2}. \tag{11}$$

It is interesting to note that Eq. (8) is identical to the second order compact filter introduced by Lele [17]. In other words, Eq. (4) can be considered as the differential counterpart of a compact filter in the continuous sense. The filter parameter $\alpha_f\in(-0.5,0.5)$ is user-defined and is used to adjust the attenuation of the filter.

The transfer function of Eq. (8) is equal to

$$T(k\Delta_\xi)=\frac{a+b\cos\left(k\Delta_\xi\right)}{1+2\alpha_f\cos\left(k\Delta_\xi\right)}. \tag{12}$$

The parameter α is determined by selecting a desired attenuation factor, α_f, which also determines $k_{1/2}$. The parameter β is determined by imposing the following constraint

$$T(k\Delta_\xi=\pi)=0. \tag{13}$$

Solving Eqs. (9) and (13) for α and β yields

$$\alpha^2=\frac{\frac{2\alpha_f}{3}-\frac{1}{6}}{1+2\alpha_f} \tag{14}$$

and

$$\beta^2=\frac{1}{12}. \tag{15}$$

It can be verified that in the case of no filtering, i.e. $\alpha=\beta$, the filtering coefficient is equal to $\alpha_f=0.5$, which is in agreement with the expected value for compact filters.

Considering that the transfer function of the differential filter in its continuous form is given by

$$T_{\mathrm{cnt}}(k)=\frac{1-\beta^2(k\Delta_\xi)^2}{1-\alpha^2(k\Delta_\xi)^2}, \tag{16}$$

it is interesting to note that the value obtained for β using the discrete transfer function is close to the value obtained from the continuous transfer function, i.e. $\beta^2=\frac{1}{\pi^2}$. It can also be verified that by increasing the order of the elements, the value of β obtained from the discrete transfer function approaches that obtained from the continuous one.

Fig. 2 shows a comparison between the spectral resolution of the proposed filter and that of Germano's filter. The transfer functions of the proposed filter, both in its continuous and discretized forms, are shown for $\alpha^2=0.0756$ and $\beta^2=1/12$. These values correspond to $\alpha_f=0.47$, which is commonly used with compact filters. The continuous transfer function reaches zero at slightly higher wavenumber, because the filter parameters were chosen using the discretized filter transfer function, rather than the continuous one.

Germano's filter parameter, δ, is chosen such that the wavenumber at which its discretized filter transfer function reaches 0.5, i.e. the filter cut-off wavenumber, $k_{1/2}$, is identical to that of the new filter in its discretized form. This ensures comparable dissipation and filter width. The transfer function of the proposed filter is essentially identical to that of a compact filter. The new filter is significantly less dissipative than Germano's filter, while completely removes the energy content at the grid cut-off wavenumber.

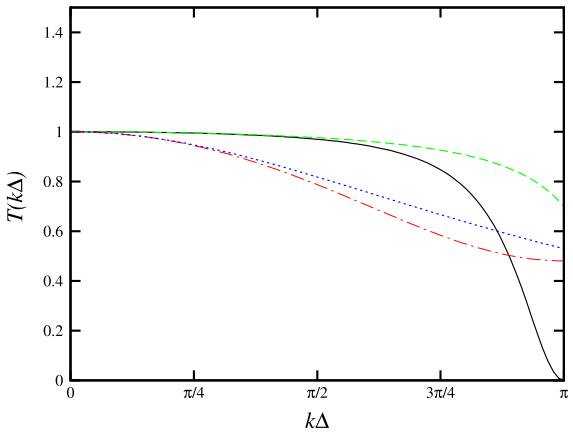

Fig. 2. Filter transfer functions in the wavenumber domain; solid line: proposed filter in discretized form, Eq. (12); dashed line: proposed filter in continuous form, Eq. (16); dashed-dotted line: Germano's filter in discretized form; dotted line: Germano's filter in continuous form, Eq. (2).

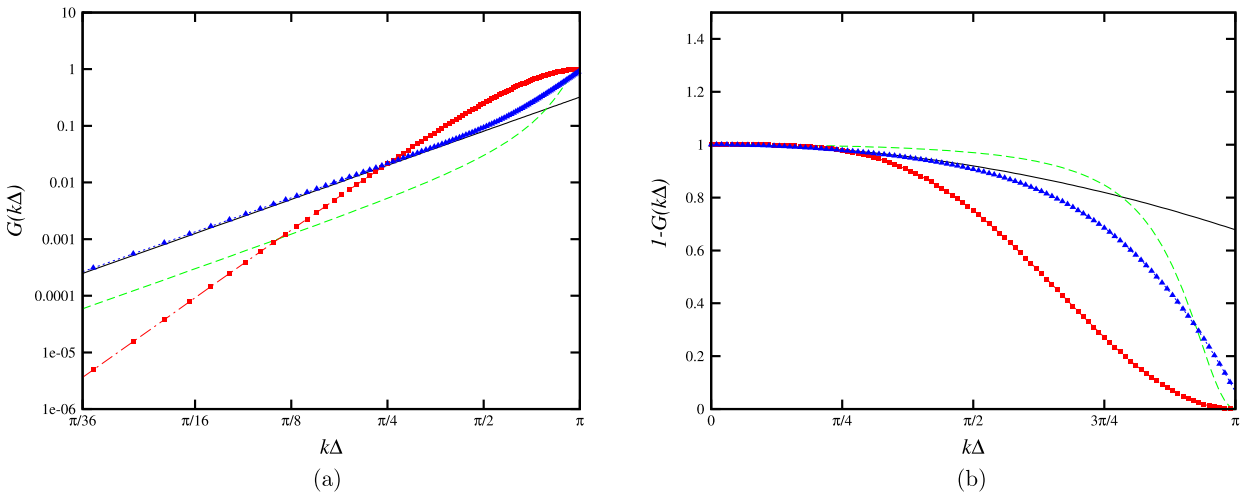

Fig. 3. Transfer function of the dissipation mechanisms (a) and filter equivalent (b) in LES; solid line: molecular viscosity given by Eq. (18); dashed line: present filter given by Eq. (19); squares: 4th order explicit filter of Bogey and Bailly given by Eq. (23); triangles: spectral eddy viscosity model given by Eq. (21).

5. Spectral accuracy of the proposed filter vs other subgrid models for LES

In this section, an a priori assessment of LES subgrid modeling using the proposed filter for approximate deconvolution modeling [8,31] or relaxation regularization [32] is presented. The analysis is based on the approach proposed by Bogey et al. [33] and Fauconnier et al. [16].

Consider the velocity attenuation due to the viscous terms. The one-dimensional equivalent of the transfer function of this term is given by [33]

$$\tilde{G}_\nu = \nu k^2 , \tag{17}$$

where k is the wavenumber. Eq. 17 can be recast in a nondimensional form to yield

$$G_\nu(k\Delta) = \frac{\tilde{G}_\nu L}{U} = \frac{1}{Re}(k\Delta)^2 \left(\frac{L}{\Delta}\right)^2 , \tag{18}$$

where U and L correspond to the characteristic flow velocity and length scale, and Δ is the grid spacing.

The one-dimensional transfer function of velocity attenuation due to the present differential filter is given by

$$G_{df}(k\Delta) = 1 - \frac{a + b\cos(k\Delta)}{1 + 2\alpha_f \cos(k\Delta)} . \tag{19}$$

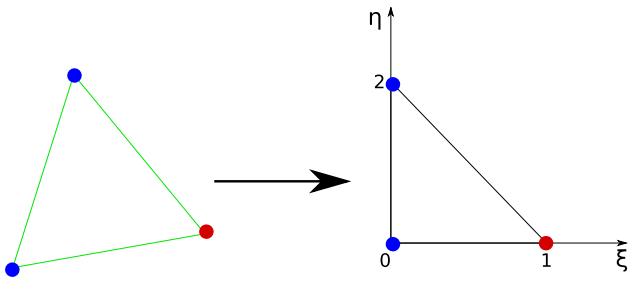

Fig. 4. Schematic illustration of triangular element transformation from the physical space (left) to a reference element in the computational space (right).

Fig. 3 shows a comparison between the dissipation, and the corresponding filtering kernels of molecular viscosity and the present filter for the LES of an isotropic turbulence at $Re = 5000$. The ratio of the characteristic length to the filter size was considered to be $\frac{L}{\Delta} = 64$. For completeness, a comparison with the attenuation of the spectral eddy-viscosity model of Chollet and Leiseur [34], and the attenuation of the explicit discrete filter of Bogey and Bailly [15,16,35] are also presented.

The one-dimensional transfer function of the spectral eddy-viscosity is given by [16,32,34]

$$\tilde{G}_{\nu,e} = \nu_e k^2 = C_k^{-3/2}\left[0.441 + 15.2e^{-3.03\frac{k_c}{c}}\right]\sqrt{\frac{E(k_c)}{k_c}}k^2\,, \tag{20}$$

where C_k is the Kolmogrov constant and is taken to be equal to 1.5 [16], k_c is the filter cutoff wavenumber, and $\tilde{E}_{k_c}$ is the spectral value of turbulent kinetic energy at the filter cutoff wavenumber. Eq. (20) can be recast in a nondimensional form to obtain

$$G_{\nu,e}(k\Delta) = \frac{\tilde{G}_{\nu,e}L}{U} = C_k^{-3/2}\left[0.441 + 15.2e^{-3.03\frac{k_c}{c}}\right]\sqrt{\frac{E(k_c)}{U^2L}\frac{1}{k_c\Delta}}\left(\frac{L}{\Delta}\right)^{3/2}(k\Delta)^2\,. \tag{21}$$

The square symbols in Fig. 3 correspond to Eq. (21) with $k_c\Delta = 0.8\pi$. The value of $E(k_c)$ was chosen using the DNS of an isotropic turbulence at the corresponding wavenumber.

The explicit filter of Bogey & Bailly is defined by

$$\bar{\phi}_i = \phi_i - \sum_{j=-n}^{n} d_j\phi_{i-j}\,, \tag{22}$$

where $d_j = -d_{-j}$ represents the weighting coefficients that determine the dissipative contribution of the $(2n+1)$-point symmetric filter with order $m = 2n$. The values of these coefficients are documented in a number of references [15,16,35] and are not repeated here. The transfer function of the explicit discrete filter of Bogey & Bailly is given by

$$G_{ef}(k\Delta) = d_0 + 2\sum_{j=1}^{n} d_j\cos(jk\Delta)\,. \tag{23}$$

The triangles in Fig. 3 correspond to the 5-point stencil (4th order) filter.

The dissipation of the present filter is clearly less than molecular viscosity dissipation for almost all wavenumbers. Only around the grid-cutoff wavenumber, the dissipation of the present filter exceeds that of molecular viscosity to completely remove energy content near the grid-cut off wavenumber. The eddy viscosity model dissipation closely follows that of the molecular viscosity over low wavenumbers and increases for wavenumbers beyond k_c. It is more dissipative than the proposed filter for almost all values of wavenumber. The explicit discrete filter of Bogey & Bailly is the most dissipative of all. It is interesting to note that the proposed filter has a much superior spectral resolution than the explicit discrete filter, despite its smaller stencil.

6. Filter design for unstructured grids

6.1. Filter design for the reference element

Consider a triangular element, Ω, in an unstructured grid. Such an element can be transformed to a reference (standard) element, $\widetilde{\Omega}$, in a two-dimensional space, (ξ, η), which is equivalent to the computational space for structured grids. This transformation is schematically shown in Fig. 4.

Using a least-square Galerkin projection, the filter equation (4) is discretized for a given element in the computational domain, $\widetilde{\Omega}$, to yield

$$\mathbf{m}\bar{\phi} = \mathbf{n}\phi\,. \tag{24}$$

The matrices in Eq. (24) are given by

$$m_{i,j} = \int_{\widetilde{\Omega}} N_i N_j \, \mathrm{d}\widetilde{\Omega} - \int_{\widetilde{\Omega}} \alpha^2 \widetilde{\nabla} N_i \cdot \widetilde{\nabla} N_j \, \mathrm{d}\widetilde{\Omega}, \tag{25}$$

and

$$n_{i,j} = \int_{\widetilde{\Omega}} N_i N_j \mathrm{d}\widetilde{\Omega} - \int_{\widetilde{\Omega}} \beta^2 \widetilde{\nabla} N_i \cdot \widetilde{\nabla} N_j \, \mathrm{d}\widetilde{\Omega}, \tag{26}$$

where N_i's are the finite element shape functions. It should be noted that Eq. (25) and (26) are evaluated in the computational domain. The operator $\widetilde{\nabla}$ also denotes the gradient operator with respect to the computational domain coordinates.

Using the following linear shape functions for triangular elements:

$$N_0(\xi, \eta) = 1 - \xi - \eta, \tag{27}$$

$$N_1(\xi, \eta) = \xi, \tag{28}$$

and

$$N_2(\xi, \eta) = \eta, \tag{29}$$

the integrals appearing in Eqs. (25) and (26) are evaluated to obtain

$$\int_{\widetilde{\Omega}} N_0 N_0 \, \mathrm{d}\widetilde{\Omega} = \frac{1}{12}, \tag{30}$$

$$\int_{\widetilde{\Omega}} N_0 N_1 \, \mathrm{d}\widetilde{\Omega} = \frac{1}{24}, \tag{31}$$

$$\int_{\widetilde{\Omega}} N_0 N_2 \, \mathrm{d}\widetilde{\Omega} = \frac{1}{24} \tag{32}$$

$$\int_{\widetilde{\Omega}} \widetilde{\nabla} N_0 \cdot \widetilde{\nabla} N_0 \, \mathrm{d}\widetilde{\Omega} = 1, \tag{33}$$

$$\int_{\widetilde{\Omega}} \widetilde{\nabla} N_0 \cdot \widetilde{\nabla} N_1 \, \mathrm{d}\widetilde{\Omega} = -\frac{1}{2}, \tag{34}$$

and

$$\int_{\widetilde{\Omega}} \widetilde{\nabla} N_0 \cdot \widetilde{\nabla} N_2 \, \mathrm{d}\widetilde{\Omega} = -\frac{1}{2}. \tag{35}$$

Using the above identities, and assuming that the coefficients α and β are piecewise constant within the element, one obtains the following equation corresponding to the filter equation for node 0:

$$\left(\frac{1}{12} - \alpha^2\right)\bar{\phi}_0 + \left(\frac{1}{24} + \frac{\alpha^2}{2}\right)\bar{\phi}_1 + \left(\frac{1}{24} + \frac{\alpha^2}{2}\right)\bar{\phi}_2 = \left(\frac{1}{12} - \beta^2\right)\phi_0 + \left(\frac{1}{24} + \frac{\beta^2}{2}\right)\phi_1 + \left(\frac{1}{24} + \frac{\beta^2}{2}\right)\phi_2. \tag{36}$$

Without loss of generality, consider a wave propagating along the ξ direction with $k_\xi = \pi$, and $k_\eta = 0$. For such wave, node 1 would be out of phase with its opposite edge, i.e. the edge 0–2. This is consistent with the definition of a saw-tooth wave presented in Section 2. It is required that the filter remove the energy content of such wave, i.e.

$$\bar{\phi}_0 = \bar{\phi}_1 = \bar{\phi}_2 = 0. \tag{37}$$

This, in turn, requires that the right hand side of Eq. (36) also vanish, i.e.

$$\left(\frac{1}{12} - \beta^2\right)\phi_0 + \left(\frac{1}{24} + \frac{\beta^2}{2}\right)\phi_1 + \left(\frac{1}{24} + \frac{\beta^2}{2}\right)\phi_2 = 0. \tag{38}$$

Noting that

$$\phi_0 = \phi_2 = -\phi_1, \tag{39}$$

Eq. (38) is solved for β to obtain

$$\beta^2 = \frac{1}{12}\,, \tag{40}$$

which is identical to the value obtained for a linear one-dimensional element. The parameter α can be determined from Eq. (9), through which the filter attenuation is adjusted.

6.2. Filter equation in the physical domain

In Section 6.1, filter design in the computational domain was discussed. In what follows, the transformation of the resulting filter from the computational domain to the physical domain is presented.

Transferring the filter from the computational domain to the physical space is accomplished using the following identities:

$$\int_{\widetilde{\Omega}} N_i N_j \,|\mathbf{J}|\, \mathrm{d}\widetilde{\Omega} = \int_{\Omega} N_i\, N_j \mathrm{d}\Omega \tag{41}$$

and

$$\int_{\Omega} \widetilde{\nabla} N_i\, \widetilde{\nabla} N_j |\mathbf{J}| \mathrm{d}\widetilde{\Omega} = \int_{\Omega} (\nabla N_i)^T \left(\mathbf{J}^{\mathbf{T}}\mathbf{J}\right) \nabla N_j \mathrm{d}\Omega\,. \tag{42}$$

The matrix $\mathbf{J}$ is the Jacobian matrix,

$$\mathbf{J} = \begin{bmatrix} \partial_\xi x & \partial_\xi y \\ \partial_\eta x & \partial_\eta y \end{bmatrix} = \begin{bmatrix} (x_1 - x_0) & (y_1 - y_0) \\ (x_2 - x_0) & (y_2 - y_0) \end{bmatrix}, \tag{43}$$

and

$$J = |\mathbf{J}| = (x_1 - x_0)\,(y_2 - y_0) - (x_2 - x_0)\,(y_1 - y_0)\,. \tag{44}$$

Using the identities above, the parameters for the filter equation in the physical domain, Eq. (3), are given by

$$h = J = |\mathbf{J}|\,, \tag{45}$$

$$\alpha_{xx} = \left[(\partial_\xi x)^2 + (\partial_\eta x)^2\right]\alpha\,, \tag{46}$$

$$\alpha_{yy} = \left[(\partial_\xi y)^2 + (\partial_\eta y)^2\right]\alpha\,, \tag{47}$$

$$\alpha_{xy} = \alpha_{yx} = \left[\partial_\xi x\, \partial_\xi y + \partial_\eta x\,, \partial_\eta y\right]\alpha\,, \tag{48}$$

$$\beta_{xx} = \left[(\partial_\xi x)^2 + (\partial_\eta x)^2\right]\beta\,, \tag{49}$$

$$\beta_{yy} = \left[(\partial_\xi y)^2 + (\partial_\eta y)^2\right]\beta\,, \tag{50}$$

and

$$\beta_{xy} = \beta_{yx} = \left[\partial_\xi x\, \partial_\xi y + \partial_\eta x\,, \partial_\eta y\right]\beta\,. \tag{51}$$

7. Numerical examples

7.1. Noisy sinusoidal pulse in one-dimensional elements

To demonstrate the effectiveness of the proposed filter, its performance in removing sawtooth waves from a one-dimensional signal was compared to that of Germano's filter. A velocity distribution of the form

$$u(x) = e^{-5x}\left[2\sin(2\pi x) + 3\sin(4\pi x) + 0.5\sin(2\pi/3x)\right] \tag{52}$$

was considered to represent some flow structures in one dimension. A uniform grid with 200 linear elements was used to represent the domain. The velocity field was further augmented with a sawtooth wave of amplitude 0.5, as shown in Fig. 5(a). The sawtooth waves represent q-waves generated because of unresolved structures or numerical errors generated at boundaries. The effectiveness of the proposed filter in removing sawtooth waves is clearly demonstrated in Fig. 5(b). Small discrepancies at the boundaries are observed because no filtering was performed on the boundary nodes.

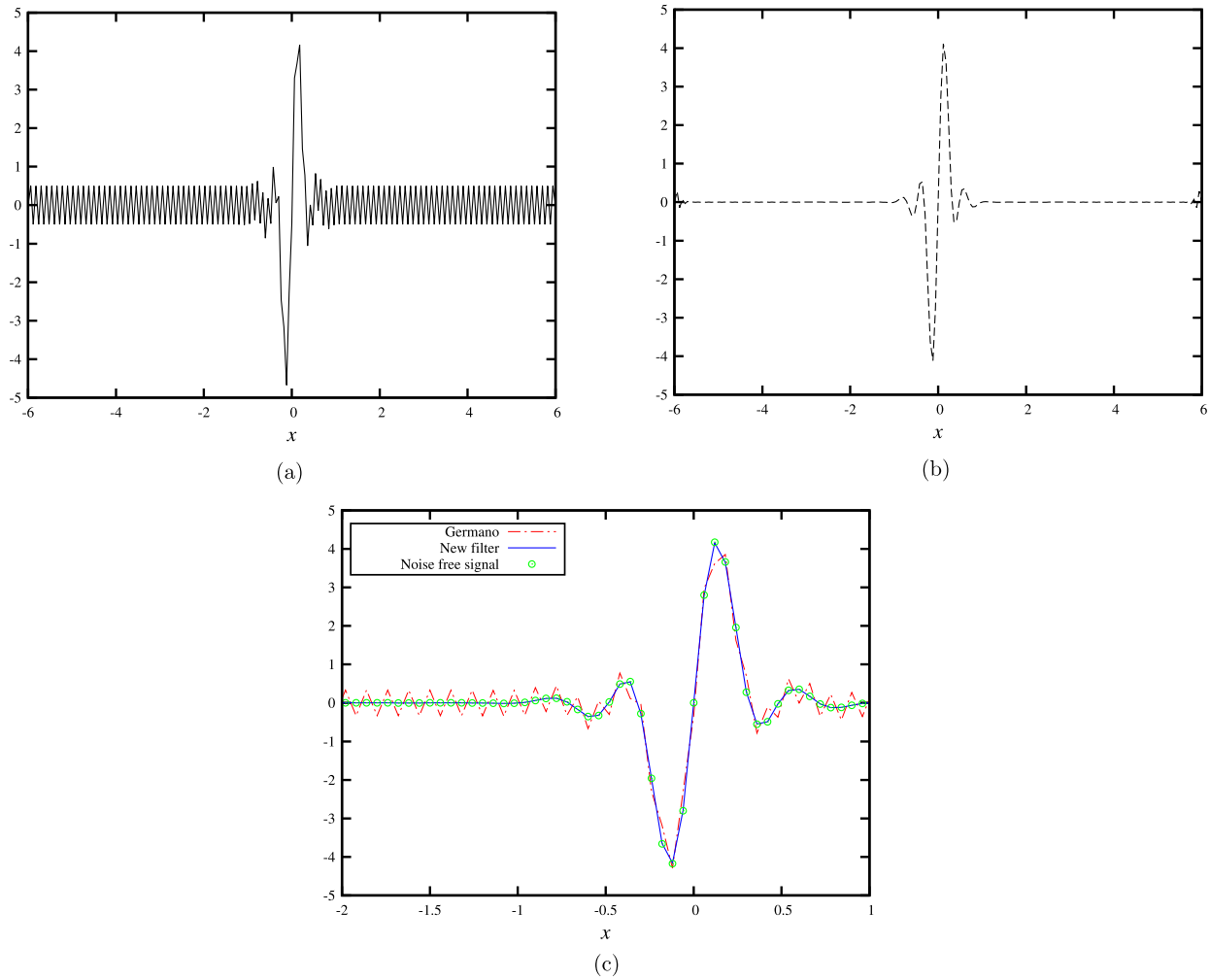

Fig. 5. Explicit filtering of a one-dimensional noisy signal on a uniform grid; (a) original signal with sawtooth waves; (b) after filtering with the proposed filter; (c) comparison with Germano's filter.

Fig. 5(c) shows a comparison between the filtered signals obtained using the new filter and that of Germano. A filter parameter $\alpha_f = 0.47$ was chosen for the proposed filter. The damping factor for Germano's filter was chosen such that both filter result in the same filter cut-off, $k_{1/2}$, wavenumber. Germano's filter did not remove the sawtooth waves from the original signal. Moreover, it caused some attenuation of the desired signal components. If left untreated, such sawtooth waves will compromise the stability of the numerical simulation.

To further demonstrate the effectiveness and stability of the proposed filter, the same problem was solved on an exponentially stretched grid. The results are shown in Fig. 6. The clustering of the sawtooth waves near the left boundary is due to the finer mesh resolution in that region. Fig. 6(b) demonstrates that the new filter completely removed the sawtooth waves from the original signal.

7.2. Saw-tooth waves on uniform and equilateral triangular elements

In order to study the performance of the proposed differential filter in two dimensions, a uniform triangular grid was generated as shown in Fig. 7(a).

A saw-tooth wave of the form

$$f(x) = \sin\left(\frac{\pi x}{h} + \frac{\pi y}{h}\right) \tag{53}$$

was imposed, where h is the grid spacing. The synthesized field and the filtered solution are shown in Fig. 7(b) and Fig. 7(c), respectively.

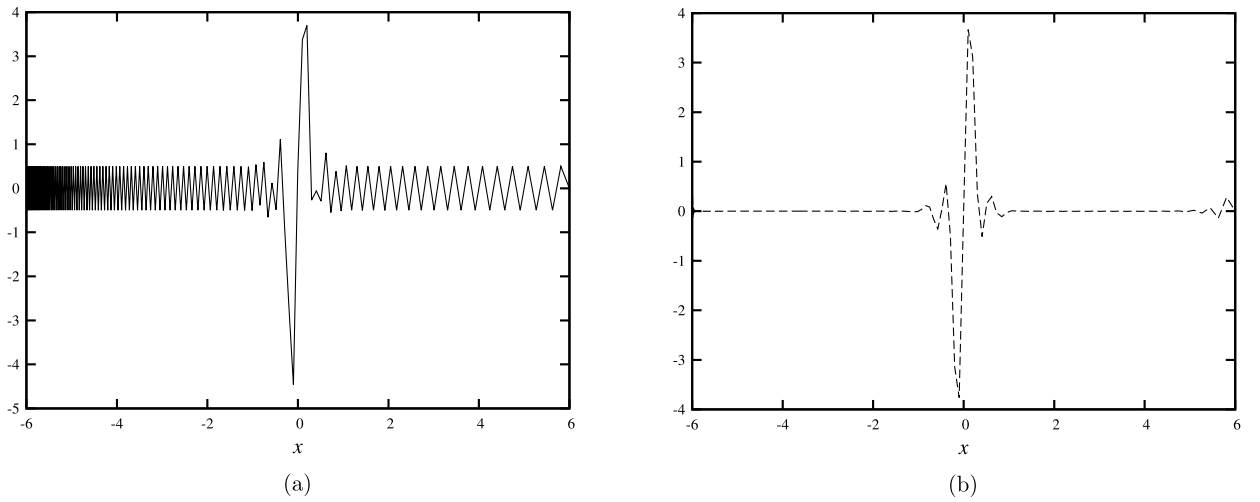

Fig. 6. Explicit filtering of a one-dimensional noisy signal on a nonuniform grid; (a) original signal with sawtooth waves; (b) after filtering with the proposed filter.

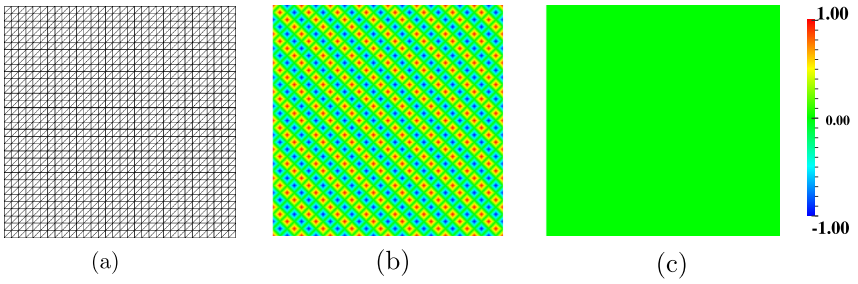

Fig. 7. Effect of filtering on uniform triangular grid; (a): the grid; (b): the imposed saw-tooth field; (c): the filtered solution.

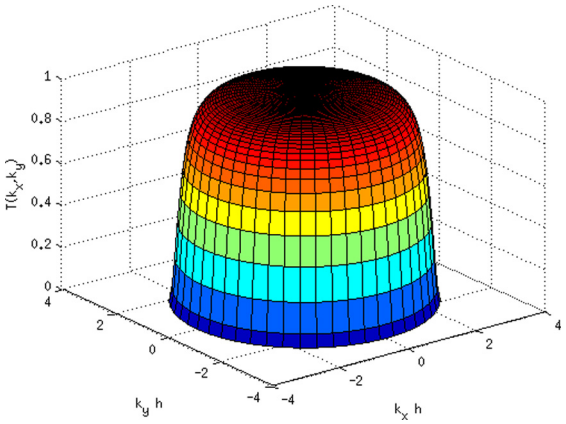

Fig. 8. The two-dimensional transfer function of the proposed filter for uniform triangular grid.

Fig. 8 shows the transfer function of the proposed filter for any node in the uniform triangular grid. The transfer function is calculated with $\alpha_f = 0.47$ as a function for $(k_x\Delta, k_y\Delta) \in [-\pi, \pi] \times [-\pi, \pi]$. The transfer function is nearly unity over a wide range of wavenumbers, before sharply declining to zero near grid cut-off.

A similar test case was performed for a grid with equilateral elements, as shown in Fig. 9. Sawtooth waves were imposed along the x-axis, and along $\theta = \pi/3$ and $\theta = \pi/6$ from the x-axis. Boundaries were considered to be periodic. Fig. 10 shows the initial field and the filtered solution. Again, the new filter completely removed the sawtooth waves regardless of their propagation direction.

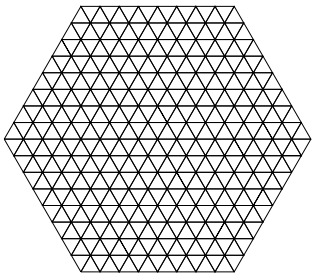

Fig. 9. Grid with equilateral triangular elements.

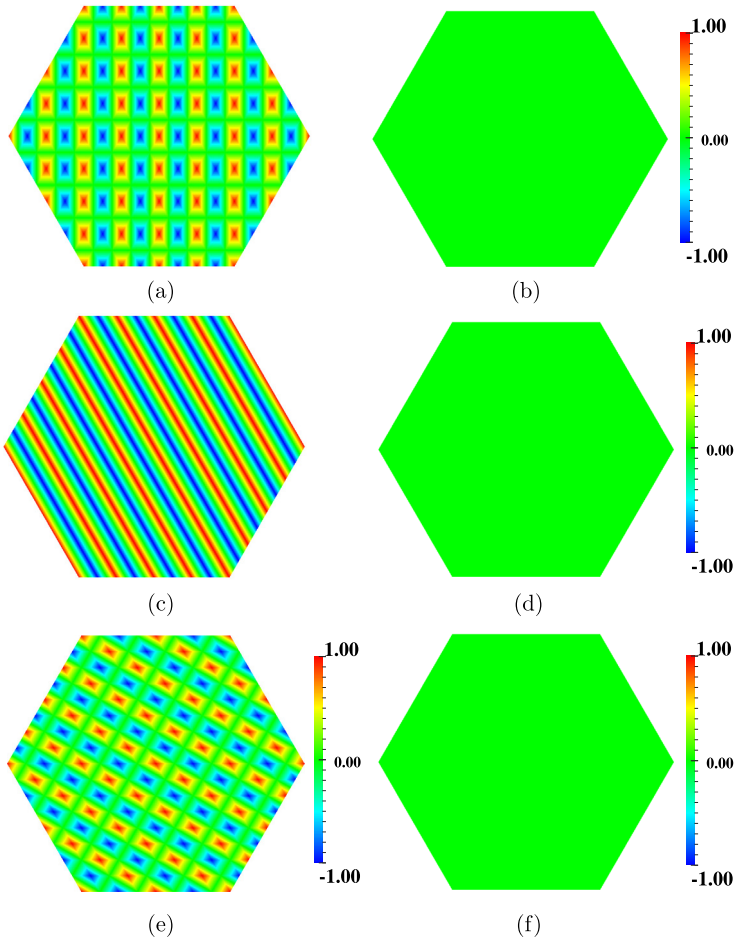

Fig. 10. Explicit filtering on equilateral triangular grid; the saw-tooth wave was aligned along (a): $x-$ axis; (c): $\theta = \pi/6$; (e): $\theta = \pi/3$; the filtered solutions are shown on the right.

7.3. Gaussian pulse with imposed fluctuations on a triangular grid

In order to further compare the performance of the proposed differential filter, a Gaussian pulse with imposed fluctuations was filtered using both methods. Fig. 11(a) shows the computational grid. The scalar field was initialized using

$$\phi = 1 + 2\exp\left(-\frac{R^2}{2R_c^2}\right) + 0.15\sin(kR)\,, \tag{54}$$

where

$$R = \sqrt{x^2 + y^2}\,. \tag{55}$$

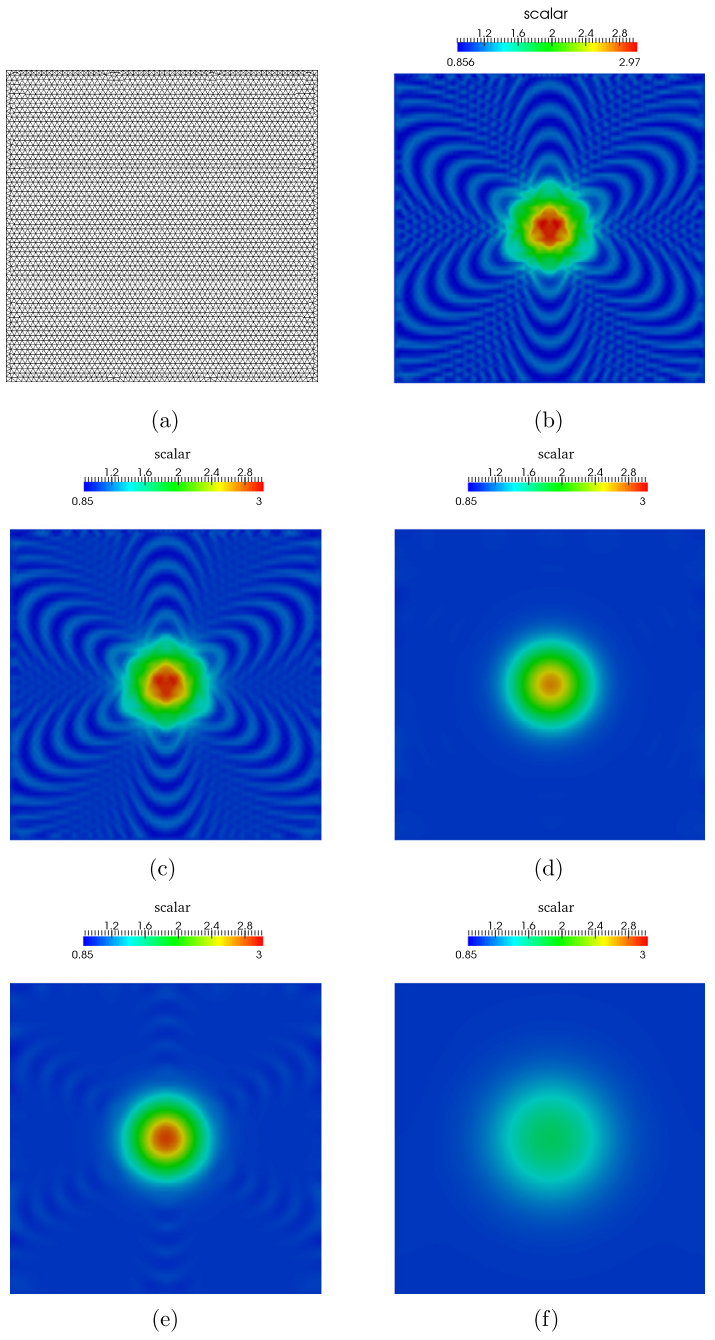

Fig. 11. Explicit filtering of Gaussian pulse with superimposed fluctuations; (a): computational grid; (b): initial field; (c): resulting field after filtering 100 times with the new filter; (d): resulting field after filtering 100 times with Germano's filter; (e): filtering 1000 times with the new filter; (f): filtering 1000 times with Germano's filter.

The exponential term in Eq. (54) provides a Gaussian pulse, while the last term on the RHS imposes a fluctuation with prescribed wavenumber k in the radial direction. Fig. 11(b) shows the imposed field with $R_c = 0.075L$ and $k\Delta = 25/3$, where the domain length is denoted by L. The mesh spacing corresponds to $\Delta = L/60$.

The use of triangular elements resulted in different sampling rates along various directions. Therefore, in some regions of the domain, the sinusoidal perturbations resulted in node to node oscillations, while sidelobes are created in some other regions. This scalar field was used as the initial input to both filters, and filtering was repeated over 1000 cycles.

The filter cut-off, $k_{1/2}$, was set to $0.9\pi/\Delta$ ($\alpha_f = 0.475$) for the proposed filter. The damping coefficient for Germano's equation was determined such that its total energy dissipation, over all wavenumbers, would be equal to that of the proposed filter.

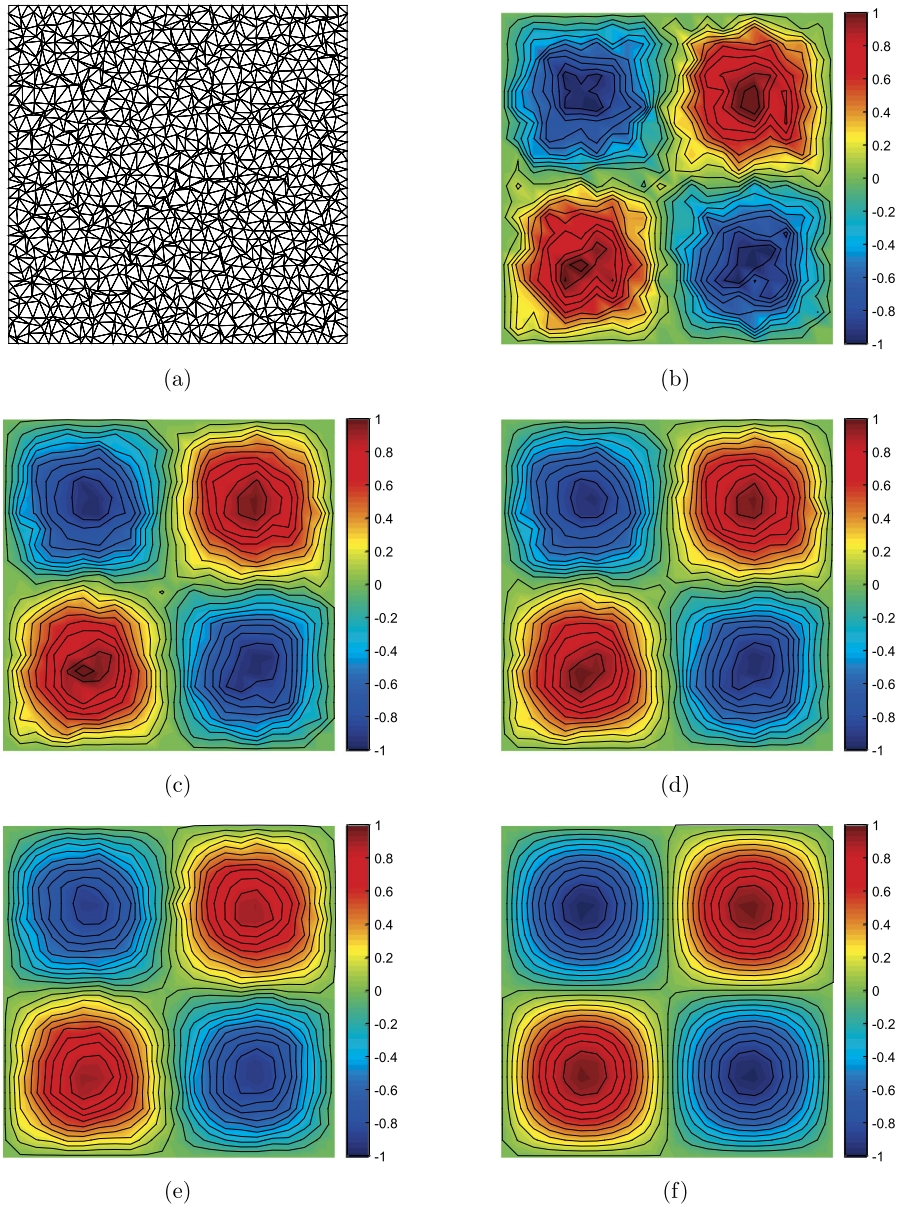

Fig. 12. Explicit filtering on a nonuniform triangular grid; (a): the grid; (b): the initial scalar field given by Eq. (57); (c): the scalar field after filtering once; (d): the scalar field after filtering twice; (d): the scalar field after filtering ten times; (e): the base field given by Eq. (56).

Filters were expected to dissipate the node to node oscillations, while still resolving the low-wavenumber field. Fig. 11(c) and 11(d) show the resulting field after 100 and 1000 times filtering with the proposed filter. Fig. 11(e) and 11(f) show the corresponding results using Germano's filter. This test case illustrates the effect of filters on turbulent structures as the simulation progresses.

The use of the proposed filter resulted in significantly improved accuracy compared to Germano's filter. After 1000 filtering cycles, the proposed filter resulted in only 8.7% attenuation of the peak value of the original Gaussian pulse, while Germano's filter resulted in 67% attenuation, suggesting that the proposed filter is better suited for LES.

7.4. Explicit filtering on a nonuniform triangular grid

The present test case is designed to investigate the effect of grid non-uniformities and the robustness of the filter to remove the high frequency content of the field on such grids. A nonuniform triangular grid with highly skewed and stretched elements, shown in Fig. 12(a), was considered. A base field with a low-wavenumber sinusoidal variation of the following form was considered:

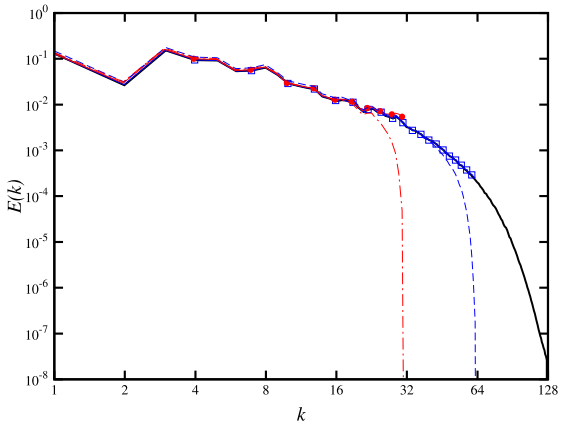

Fig. 13. The energy spectrum of a Taylor–Green vortex DNS on 256^3 grid (solid line), under-resolved DNS on 128^3 grid (squares), under-resolved DNS on 64^3 grid (circles), the filtered DNS on 128^3 grid (dashed line), and the filtered DNS on 64^3 grid (dashed-dotted line).

$$\phi(x, y) = \sin\left(\frac{2\pi x}{L}\right)\sin\left(\frac{2\pi y}{L}\right), \tag{56}$$

where L is the domain length. The average edge length of the grid was approximately equal to $L/32$. The sum of two perturbations with wavelength $L/12$ and $L/16$ (shortest resolvable wavelength) was added. The perturbations had amplitudes equal to 0.125 and 0.25 times the base signal amplitude, respectively. The resulting field was initialized using the following equation:

$$\begin{aligned}\phi(x, y) = {} & \sin\left(\frac{2\pi x}{L}\right)\sin\left(\frac{2\pi y}{L}\right) + 0.25\sin\left(16\frac{2\pi x}{L}\right)\sin\left(16\frac{2\pi y}{L}\right) \\ & 0.125\sin\left(12\frac{2\pi x}{L}\right)\sin\left(12\frac{2\pi y}{L}\right).\end{aligned} \tag{57}$$

Fig. 12 compares the initial perturbed scalar field, the scalar field after filtering, and the base solution. The filter proves to be very effective in removing perturbations without distorting or significantly dissipating the base field. In fact, it was observed that even after filtering 10 times, the peak value of the base solution was dissipated by only 7%, despite the fact that the grid was highly skewed.

7.5. A-priori analysis for LES modeling

In order to investigate the performance of the proposed filter for LES, an *a-priori* analysis of explicit filtering modeling for LES using the proposed filter was performed. The Direct Numerical Simulation of a Taylor–Green vortex transition to isotropic turbulence was considered. The DNS result was obtained using a structured compressible Navier–Stokes solver using the 6th order compact scheme [17] for the spatial discretization, the standard 4th order Runge–Kutta scheme for temporal discretization, and an 11th order compact spatial filter to eliminate aliasing [36]. The DNS solution was obtained using a structured grid with 256^3 grid points. The solution at the non-dimensional time $t = 9$ was used for the purpose of this *a-priori* analysis.

The DNS solution was used to interpolate the turbulent velocity field on two coarser grids with 128^3 and 64^3 grid points to obtain under-resolved solutions. The hexahedral elements of 64^3 and 128^3 structured grids were then broken into tetrahedral elements for filtering operations using the proposed filter.

Fig. 13 compares the energy spectrum of the filtered DNS against under-resolved DNS as well as the full DNS spectrums. It can be observed that the new filter preserves the energy content for wavenumbers smaller than the grid cut-off. The sharp drop near the grid cut-off wavenumber completely removes the under-resolved energy content. The results suggest that the proposed differential filter can be effectively used for high-resolution LES of turbulent flows.

8. Conclusions

A high resolution low-pass differential filter is proposed for unstructured grids. The discrete differential filter is derived for finite element methods in one- and two-dimensional domains. Suitable constraint equations are defined to ensure that the filter vanishes at the grid cut-off frequency, and to allow the choice of the filter attenuation.

The proposed filter reduces to a compact filter for structured grids, implying that it can be considered as the differential counterpart of compact filters. The design procedure introduced in this work may easily be used with other discretization schemes (e.g. finite volume) which will be pursued in future works.

A number of benchmarks with synthesized solutions are presented to illustrate the performance of the proposed discrete differential filter. It is shown that the proposed filter results in significantly improved accuracy compared to Germano's differential filter. Using a test case on a two-dimensional unstructured grid, it was observed that even after 1000 filtering cycles, the proposed filter resulted in only 8.7% attenuation, while Germano's filter resulted in 67% attenuation of the original signal.

An *a priori* analysis of filtered DNS data further suggest the suitability of the proposed filter for LES. Future work will include application of the proposed filter in an explicit filtering LES, and an investigation of its performance for turbulence statistics.

Acknowledgements

This work was sponsored in part by the Green Aviation Research and Development Network (GARDN) through Pratt and Whitney Canada, the National Science and Engineering Research Council (NSERC) of Canada.

References

[1] S.B. Pope, Turbulent Flow, Cambridge University Press, 2000.
[2] T.S. Lund, The use of explicit filters large eddy simulation, Comput. Math. Appl. 46 (2003) 603–616.
[3] A.G. Kravchenko, P. Moin, Numerical studies of flow over a circular cylinder at Re = 3900, Phys. Fluids 12 (2) (2000) 403–417.
[4] J. Meyers, P. Sagaut, Is plane-channel flow a friendly case for the testing of large-eddy simulation subgrid-scale models?, Phys. Fluids 19 (4) (2007) 048105.
[5] T.S. Lund, H.-J. Kaltenbach, Experiments with explicit filtering for LES using a finite-difference method, in: Annual Research Briefs, Center for Turbulence Research, 1995, pp. 91–105.
[6] O.V. Vasilyev, T.S. Lund, P. Moin, A general class of commutative filters for LES in complex geometries, J. Comput. Phys. 146 (1) (1998) 82–104.
[7] N. Adams, S. Stolz, A subgrid-scale deconvolution approach for shock capturing, J. Comput. Phys. 178 (2) (2002) 391–426.
[8] S. Stolz, N.A. Adams, L. Kleiser, An approximate deconvolution model for large-eddy simulation with application to incompressible wall-bounded flows, Phys. Fluids 13 (4) (2001) 997.
[9] S. Stolz, A. Adams, L. Kleiser, The approximate deconvolution model for compressible flows: isotropic turbulence and shock-boundary-layer interaction, in: R. Friedrich, W. Rodi (Eds.), Advances in LES of Complex Flows, Kluwer Academic Publishers, Netherlands, 2002, pp. 33–47.
[10] N.A. Adams, A stochastic extension of the approximate deconvolution model, Phys. Fluids 23 (5) (2011) 055103.
[11] J. Mathew, R. Lechner, H. Foysi, J. Sesterhenn, R. Friedrich, An explicit filtering method for large eddy simulation of compressible flows, Phys. Fluids 15 (8) (2003) 2279.
[12] C. Bogey, C. Bailly, Computation of a high Reynolds number jet and its radiated noise using large eddy simulation based on explicit filtering, Comput. Fluids 35 (10) (2006) 1344–1358.
[13] C. Bogey, C. Bailly, Large eddy simulations of round free jets using explicit filtering with/without dynamic Smagorinsky model, Int. J. Heat Fluid Flow 27 (4) (2006) 603–610.
[14] S.T. Bose, P. Moin, D. You, Grid-independent large-eddy simulation using explicit filtering, Phys. Fluids 22 (10) (2010) 105103.
[15] J. Berland, P. Lafon, F. Daude, F. Crouzet, C. Bogey, C. Bailly, Filter shape dependence and effective scale separation in large-eddy simulations based on relaxation filtering, Comput. Fluids 47 (1) (2011) 65–74.
[16] D. Fauconnier, C. Bogey, E. Dick, On the performance of relaxation filtering for large-eddy simulation, J. Turbul. 14 (1) (2013) 22–49.
[17] S.K. Lele, Compact finite difference schemes with spectral-like resolution, J. Comput. Phys. 103 (1) (1992) 16–42.
[18] M.R. Visbal, D.P. Rizzetta, Large-eddy simulation on curvilinear grids using compact differencing and filtering schemes, J. Fluids Eng. 124 (4) (2002) 836.
[19] D.P. Rizzetta, M.R. Visbal, G.A. Blaisdell, A time-implicit high-order compact differencing and filtering scheme for large-eddy simulation, Int. J. Numer. Methods Fluids 42 (2003) 665–693.
[20] A. Uzun, M.Y. Hussaini, Simulation of noise generation in the near-nozzle region of a chevron nozzle jet, AIAA J. 47 (8) (2009) 1793–1810.
[21] A. Uzun, J. Bin, M.Y. Hussaini, High-fidelity numerical simulation of a chevron nozzle jet flow, Int. J. Aeroacoust. 10 (5&6) (2011) 531–564.
[22] A.L. Marsden, O.V. Vasilyev, P. Moin, Construction of commutative filters for LES on unstructured meshes, J. Comput. Phys. 175 (2) (2002) 584–603.
[23] A. Haselbacher, O.V. Vasilyev, Commutative discrete filtering on unstructured grids based on least-squares techniques, J. Comput. Phys. 187 (1) (2003) 197–211.
[24] S.T. Bose, P. Moin, F. Ham, Explicitly filtered large eddy simulation on unstructured grids, in: Annual Research Briefs, Center for Turbulence Research, 2011, pp. 87–96.
[25] M. Germano, Differential filters for the large eddy numerical simulation of turbulent flows, Phys. Fluids 29 (6) (1986) 1755.
[26] M. Germano, Differential filters of elliptic type, Phys. Fluids 29 (6) (1986) 1757.
[27] J.S. Mullen, P.F. Fischer, Filtering techniques for complex geometry fluid flows, Commun. Numer. Methods Eng. 15 (1999) 9–18.
[28] D. You, S.T. Bose, P. Moin, Grid-independent large-eddy simulation of compressible turbulent flows using explicit filtering, in: Annual Research Briefs, Center for Turbulence Research, 2010, pp. 203–210.
[29] W.J. Layton, L.G. Rebholz, Approximate Deconvolution Models of Turbulence, Springer-Verlag, Berlin, Heidelberg, 2011.
[30] R. Vichnevetsky, J.B. Bowles, Fourier Analysis of Numerical Approximations of Hyperbolic Equations, vol. 5, Siam, 1982.
[31] S. Stolz, N. Adams, An approximate deconvolution procedure for large-eddy simulation, Phys. Fluids 11 (1999) 1699.
[32] S.B. Müller, N.A. Adams, L. Kleiser, S.B. Muller, N.A. Adams, L. Kleiser, Analysis of relaxation regularization as subgrid-scale model for large-eddy simulation, in: Direct and Large-Eddy Simulation V, Springer-Verlag, 2004, pp. 57–64.
[33] C. Bogey, O. Marsden, C. Bailly, Large-eddy simulation of the flow and acoustic fields of a Reynolds number 10^5 subsonic jet with tripped exit boundary layers, Phys. Fluids 23 (3) (2011) 035104.
[34] J.-P. Chollet, M. Lesieur, Parameterization of small scales of three-dimensional isotropic turbulence utilizing spectral closures, J. Atmos. Sci. 38 (12) (1981) 2747–2757.
[35] C. Bogey, C. Bailly, A family of low dispersive and low dissipative explicit schemes for flow and noise computations, J. Comput. Phys. 194 (1) (2004) 194–214.
[36] A. Najafi-Yazdi, Large eddy simulation of sound generation by turbulent reacting and nonreacting shear flows, Dissertation, McGill University, 2011.